Mechanics of Microtubules: Effects of Protofilament Orientation

Zachary J. Donhauser,* William B. Jobs, and Edem C. Binka
Department of Chemistry, Vassar College, Poughkeepsie, New York

ABSTRACT Microtubules are hollow cylindrical polymers of the protein tubulin that play a number of important dynamic and structural roles in eukaryotic cells. Both in vivo and in vitro microtubules can exist in several possible configurations, differing in the number of protofilaments, helical rise of tubulin dimers, and protofilament skew angle with respect to the main tube axis. Here, finite element modeling is applied to examine the mechanical response of several known microtubule types when subjected to radial deformation. The data presented here provide an important insight into microtubule stiffness and reveal that protofilament orientation does not affect radial stiffness. Rather, stiffness is primarily dependent on the effective Young's modulus of the polymerized material and the effective radius of the microtubule. These results are also directly correlated to atomic force microscopy nanoindentation measurements to allow a more detailed interpretation of previous experiments. When combined with experimental data that show a significant difference between microtubules stabilized with a slowly hydrolyzable GTP analog and microtubules stabilized with paclitaxel, the finite element data suggest that paclitaxel increases the overall radial flexibility of the microtubule wall.

INTRODUCTION

Microtubules are one of the essential components responsible for the structural and spatial organization of eukaryotic cells. Their significant roles in many essential cellular functions are well known: they are part of the machinery that conducts mitosis and meiosis, they participate in directed intracellular transport, and they have an integral role as part of the cytoskeleton (1). Because of their fundamental structural purpose, a complete grasp of the various factors that impact microtubule mechanical properties is key to a full understanding of their function.

For this reason, there has been considerable interest in the rigidity of microtubules. The significant majority of microtubule mechanical studies have relied on optical microscopy to observe bending of whole microtubules and directly measure flexural rigidity, with bending induced by techniques such as thermal fluctuations, optical tweezers, and fluid flow. However, despite the large number of microtubule bending studies that have been reported, there is no consensus value for microtubule flexural rigidity, with values ranging over an order of magnitude from 3.7×10^{-24} to 35.8×10^{-24} $N \cdot m^2$ for paclitaxel-free microtubules and from 1.0×10^{-24} to 32×10^{-24} $N \cdot m^2$ for paclitaxel-stabilized microtubules (2–12). The rigidity values differ not only because of the different experimental methods used, but also because of subtle variations in microtubule assembly conditions or solution conditions.

Recently, we and other groups have explored the use of atomic force microscopy (AFM) to study other modes of microtubule deformation, such as radial indentation (13–17) and localized bending (18,19). AFM provides a unique approach because it is able to probe microtubules locally, inducing different modes of deformation than in bending experiments. We previously used AFM to compare the structural and mechanical properties of paclitaxel-stabilized microtubules with those polymerized in the presence of guanylyl-(α, β)-methylene-diphosphonate (GMPCPP), another stabilizing agent (14). In those experiments we found significant differences in both morphology and radial stiffness between paclitaxel- and GMPCPP-stabilized microtubules, which could plausibly be caused by changes in the material properties of the tubulin polymer (e.g., effective Young's modulus) or in the microtubule structure. There are several structural motifs that differ between paclitaxel- and GMPCPP-stabilized microtubules and could impact their radial stiffness, including variations in protofilament number, tubulin helical rise, and protofilament orientation.

To investigate the relative mechanical changes induced by microtubule structural motifs and explore the indentation of microtubules more fully, we employed finite element modeling (FEM) to examine several known microtubule types and determine their mechanical response to radial deformation. FEM is a common method of choice for describing the mechanics of biological systems, including cells (20,21), viral particles (22–24), macromolecules (25), and lipid nanotubes (26), at the micrometer and nanometer scales. Of relevance to work presented here, several studies have used FEM (e.g., in nanoscopic bending (19,27) and radial indentation (13,15) experiments) to interpret deformation of microtubules. Here, we use FEM to describe the relative effects of microtubule radius and protofilament skew on radial indentation experiments conducted with AFM, with a focus on interpreting experimentally observed differences in the effective radial spring constant of the microtubule wall (k_{MT}) in different microtubule types. The results presented are then applied more broadly to address the long-range effects of stabilization with paclitaxel.

Submitted January 8, 2010, and accepted for publication June 25, 2010.

*Correspondence: zadonhauser@vassar.edu

Editor: Marileen Dogterom.

0006-3495/10/09/1668/8 $2.00

doi: 10.1016/j.bpj.2010.06.065

Microtubule structure

Because variability of structure across different microtubule types is central to this work, we provide a brief overview here. Microtubule structure is well established (28–30): heterodimers of the protein tubulin are associated longitudinally into protofilaments, and eight to 17 protofilaments associate laterally to form the hollow microtubule cylinder (31). Microtubule assembly aligns protofilaments approximately parallel to the main microtubule axis, with adjacent protofilaments slightly offset longitudinally (by ~1 nm), resulting in a microtubule lattice that is a pseudohelix of tubulin dimers.

Within this general structural blueprint, both in vivo and in vitro microtubules can assemble into a wide range of different configurations (31–35), each characterized by a unique number of protofilaments (*N*) and/or helix start number (*S*). These different microtubule types (labeled using the configuration *N_S*) adopt varying degrees of protofilament skew relative to the main microtubule longitudinal axis to maintain favorable tubulin-tubulin interactions (28). Skew angles are generally restricted to $<2^\circ$ because of the significant bending required in the protofilaments for skew angles outside of this range. All known microtubule types adopt skewed protofilament geometries, with the exception of the 13_3 microtubule. A schematic of a skewed microtubule lattice is depicted in Fig. 1 *A*, in which α- and β-tubulin monomers are labeled and a single protofilament is highlighted.

The microtubules found in vivo are most frequently 13_3, although this can vary across species and cellular conditions (31,36,37). Several studies (33,34,38–43) have shown that the principal *N_S* microtubule configuration is sensitive to both assembly and stabilization conditions in vitro. For example, assembly of microtubules in the presence of paclitaxel results in a population of microtubules in which 12_3 is the most common type (38–41). More recent evidence also suggests that paclitaxel can drive the rearrangement of microtubules from mostly 13_3 to mostly 12_3 when the drug is added to preassembled microtubule samples (41). Whereas paclitaxel reduces the protofilament number, GMPCPP induces an increase in the average protofilament number. Assembly of microtubules in the presence of this slowly hydrolyzing nucleotide analog can result in microtubule populations with >95% 14_3 microtubules (43).

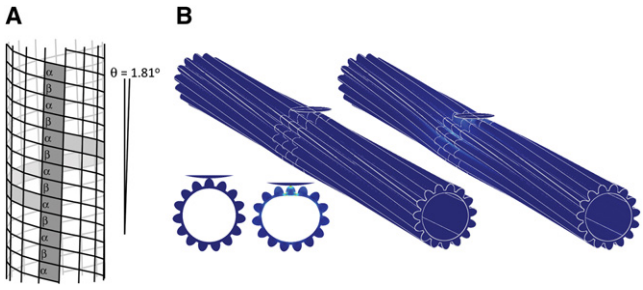

FIGURE 1 Representations of a skewed microtubule lattice. (*A*) Schematic of a 15_4 microtubule, highlighting a single protofilament in dark gray, which is skewed 1.81° with respect to the main longitudinal axis of the microtubule. A single helical turn is highlighted in light gray. (*B*) The same type of 15_4 microtubule, 500 nm in length, as described for FEM. Depicted are the initial model (*left*) and after 3 nm of indentation (*right*). In the indented microtubule, lighter shades of blue indicate regions of high stress. Inset: Cross-sections of the tubes before and after indentation, with stress indicated by color.

MATERIALS AND METHODS

Finite element modeling

All finite element calculations were performed using COMSOL Multiphysics 3.4 (COMSOL, Burlington, MA). To establish basic scaling relationships in simple, three-dimensional geometries, for the initial models we employed a set of thick-shelled cylinders without protofilaments, with varying inner radii (8–11 nm) and wall thicknesses (0.5–2.0 nm), using a linear, isotropic material with a Young's modulus (*E*) of 0.6 GPa. This value was chosen based on previous FEM studies (13,15) and because for realistic geometries it produces values for k_{MT} that correlate well with experimental data. The tubes were immobilized on the bottom along their length and subjected to radial indentation from the top with parabolic tips. These models were useful for comparison with previously reported FEM studies (13,15) and for determining the appropriate meshing parameters and element sizes to achieve more realistic microtubule models.

Protofilament-containing microtubule models were constructed with the same material properties, with a cross-sectional geometry as depicted in the inset of Fig. 1 *B*. This cross-section was used based on previous FEM studies of microtubules (13,15,16) and is an approximation of the microtubule cross-section determined using crystallographic and cryoelectron microscopy data, which showed a lateral association between protofilaments through thin bridges of ~1 nm thickness, a roughly corrugated outer surface, and a relatively smooth inner surface (28–30). The basis for the microtubule body was a 1.1 nm thick cylindrical shell, with a radius that depended on the number of protofilaments. Protofilament cross-sections were defined as hemi-ellipses protruding 3 nm from the main tube shell, providing the microtubule cross-section with a total thickness of 4.1 nm at the thickest part of the protofilament. The *N* protofilaments were spaced equally around the outer radius of the main shell at a distance of $360^\circ/N$. In accord with previously published FEM studies (15,19), the substrate underlying the microtubule in an AFM experiment was modeled by fixing the position of the bottommost surface(s) of the tube. The average radii of the cylindrical shells were selected based on published effective microtubule radii (35). The average radius (R_{avg}) was calculated numerically using the outer radius and inner radius (R_{in}) of the shell cross-section at all radial angles. The average radius values ranged from 8.27 nm for a 10_2 microtubule to 12.17 nm for a 15_4 microtubule and are listed in Table 1. Three-dimensional microtubule models were produced by extruding the

TABLE 1 Summary of microtubule types modeled

type	*t* (nm)	R_{avg} (nm)	R_{in} (nm)	Skew (°)	k_{MT} (N/m)
10_2	2.75	8.27	6.90	−1.5	0.114
11_2a	2.82	8.82	7.42	−2.11	0.104
11_2b	2.80	8.89	7.50	−0.53	0.103
12_2	2.76	10.01	8.64	−1.02	0.081
12_3	2.73	10.18	8.81	0.85	0.077
13_3	2.79	10.72	9.32	0	0.073
14_4	2.83	11.35	9.94	0.87	0.067
14_3	2.79	11.59	10.19	−0.68	0.063
15_4	2.83	12.17	10.75	1.81	0.060
15_3	2.84	12.19	10.78	−1.33	0.060

cross-section to a total length of 500 nm. Protofilament skew was introduced using a twist operation during the extrusion. Skew angles used in this study were based on reported values and are reported in Table 1 (33,35). Whenever possible, we took advantage of symmetry (e.g., for a 13_3 microtubule) and reduced the model size to a quarter tube.

The AFM tip was modeled as a rigid ($E = 2 \times 10^{11}$ GPa) paraboloid with a radius of 20 nm positioned at the center of the microtubule. To induce microtubule indentation, the tip position was offset radially into the tube, and contact between the tip and microtubule was modeled using a standard contact penalty method (15). In this method, the contact pressure varies exponentially with gap distance between the tip and tube, and when it is in intimate contact the surface of the softer tube obeys the boundary established by the much stiffer tip. The total force was obtained by integrating the vertical component of the load over the contact area. The final whole microtubule models consisted of 80,000–100,000 elements, with element dimensions ranging from ~0.5 nm near the tip-microtubule contact to ~5 nm in regions at the microtubule ends.

Atomic force microscopy

For the representative AFM data presented below, preparation of GMPCPP- and paclitaxel-microtubule solutions and AFM was performed as previously described (14). Briefly, aqueous microtubule solutions (final tubulin concentration: 0.2–40 μg/mL) were dropped on amine-silanized mica sheets (Ted Pella, Redding, CA). AFM imaging and force data collection were performed using a Veeco Multimode/Nanoscope IIIa (Veeco Metrology, Santa Barbara, CA) operating in tapping mode under buffer. During force-data collection, tip oscillation was turned off and cantilever deflection was recorded as a function of sample z-position during tip-sample approach and retraction. Flexible silicon nitride cantilevers with nominal spring constants of 0.06 N/m (NP or NP-S cantilevers; Veeco Metrology, Santa Barbara, CA) were used and calibrated by the reference cantilever method (44). Raw data containing cantilever deflection as a function of distance were converted to indentation as a function of distance by comparison with cantilever sensitivity curves collected on bare mica after each experiment.

RESULTS AND DISCUSSION

In previous AFM experiments we examined paclitaxel- and GMPCPP-stabilized microtubules and found average values of effective radial spring constant (k_{MT}) of 0.07 $\pm$ 0.03 N/m and 0.17 $\pm$ 0.05 N/m, respectively, for the two types (14). Here, we provide representative indentation data from AFM experiments on paclitaxel- and GMPCPP-stabilized microtubules for comparison with modeling data. The force data are depicted in Fig. 2, with approach data shown in blue and retraction data shown in green. The application of low force (Fig. 2, *A* and *B*) results in elastic indentation and reveals the effective spring constant (k_{MT}) as the slope of the indentation region. Fig. 2, *A* and *B* shows indentation of a paclitaxel- and a GMPCPP-microtubule with k_{MT} of 0.076 N/m and 0.197 N/m, respectively. These values are representative of the many indentation experiments performed on the two types of microtubules (14). Subsequent application of higher force to the same GMPCPP-microtubule results in an abrupt discontinuity in the force-indentation curve, which is associated with buckling of the microtubule under the applied load. After the tube collapses completely, the force rises without additional indentation,

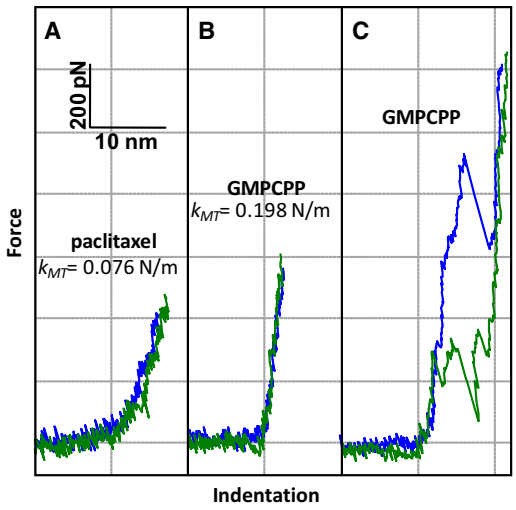

FIGURE 2 Force-versus-indentation plots during tip approach (*blue*) and retraction (*green*). Shown here are representative curves for (*A*) a paclitaxel microtubule and (*B*) a GMPCPP-microtubule. In both *A* and *B*, a nearly linear elastic response is observed during application of low force. (*C*) Application of higher force to the same GMPCPP microtubule results in discontinuities corresponding to tube collapse or rupture.

indicating that the AFM tip is in contact with the mica beneath the microtubule. Retraction curves (indicated in *green*) show similar discontinuities, although at lower force. Reimaging of the same microtubule can reveal whether these retraction discontinuities represent full or partial restoration of the microtubule cylinder. Our FEM models describe elastic indentation, as in Fig. 2, *A* and *B*, but do not accurately describe the highly nonlinear buckling events shown in Fig. 2 *C*.

A physical description of radial indentation of microtubules by AFM was provided by de Pablo et al. (13) and Schaap et al. (15), who used a combination of an analytical description of thin-walled cylinders and FEM to describe the relationship between the effective spring constant of the microtubule wall, k_{MT}, and the effective Young's modulus of the microtubule, E, as:

$$\frac{k_{MT}}{ER} \cong C\left(\frac{t}{R}\right)^n \tag{1}$$

where R is the tube radius and t is the wall thickness. C is a dimensionless prefactor that varies based on the specific boundary conditions and tube geometry, and n is a scaling exponent. For tubes with negligible wall thickness, symmetrical indentation with point forces yields $C \approx 1$ and $n = 3/2$. Thin-shell FEM was used to validate our results against previous work (15) and to verify that this relationship applies to asymmetric indentation, where the tube is supported along its length underneath and indented from above (data not shown).

To address the differences in k_{MT} between paclitaxel- and GMPCPP-stabilized microtubules, our initial FEM models

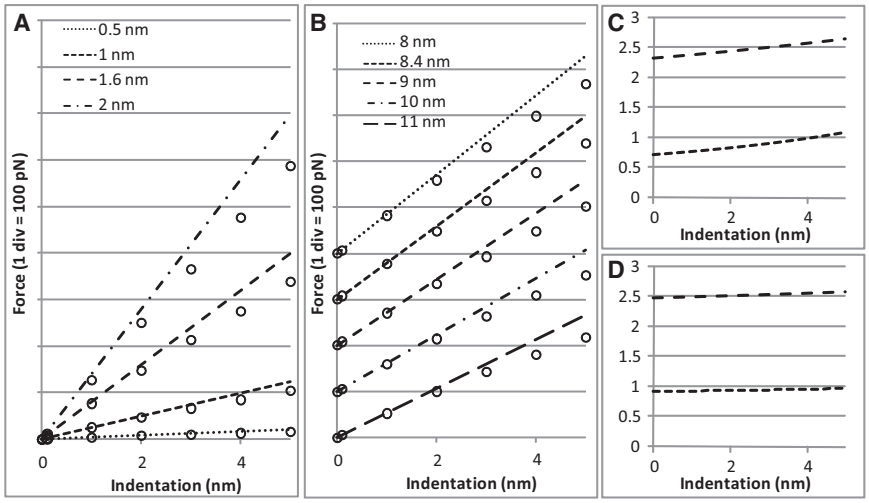

FIGURE 3 Response of thick-walled tubes to asymmetric radial indentation. Tubes of varying thicknesses (*A* and *C*) and radii (*B* and *D*) were indented up to 5 nm and the scaling relationships were examined. (*A*) Force versus indentation for tubes of the thicknesses indicated, each with an inner radius of 8.4 nm. Slopes of the lines were calculated from Eq. 1. (*B*) Force versus indentation for tubes of radii indicated and $t = 1.6$ nm (offset for clarity). (*C*) Least-squares fitting of the data from *A* to Eq. 1, showing variation in the exponent, n (~2.5), and prefactor, C (~0.7-1), as a function of indentation depth. (*D*) Least-squares fitting of the data from *B*.

focused on the effect of changing the wall thickness (t) and tube radius (R). Some deviations from Eq. 1 are expected for tubes with finite wall thickness indented with finite-sized tips. Factors that cause deviations from thin-shell behavior can be grouped into two categories: those that lead to relative stiffening of the tube and an increase in k_{MT} relative to Eq. 1, and those that lead to a relative softening of the tube and a decrease in k_{MT}. Of relevance to our experiments, it was previously reported that stiffening may arise from the finite contact area of the indenting tip or underlying substrate, and softening can arise from compression of the tube wall, buckling of the tube, or bending of protofilaments out of the tube wall (15). During indentation of the tube, the net deviation from Eq. 1 is determined by the balance of factors that lead to softening and stiffening for a specific geometry. We evaluated these effects in geometries comparable to AFM experiments, modeling indentation for a series of thick-walled tubes ($t = 0.5$–2.0 nm, $R = 8$–11 nm) indented by a 20 nm parabolic tip. The results of these models are shown in Fig. 3.

In actual AFM experiments, the total amount of indentation that is possible is limited by tube collapse, which typically occurs with small indentations (<5 nm). Thus, to examine the precollapse, elastic indentation region, indentation is only modeled up to 5 nm. For indentation up to 5 nm of thick-walled tubes with dimensions comparable to microtubules, deviation from Eq. 1 is dominated by wall compression, leading to a net softening effect (Fig. 3, *A* and *B*), and a lower slope than expected in comparison with thin-walled tubes. The absolute magnitude of this effect is only slightly more significant in tubes with larger radii, yet it depends more markedly on wall thickness in our models.

Even with this deviation, the thick-shell indentation data show the validity of using a thin-shell approximation to describe indention of microtubules. Although the indentation curves are slightly nonlinear, k_{MT} can be approximated as the average slope at each indentation depth. The scaling relationships between k_{MT} and R and t were examined by fitting to Eq. 1 to determine the effective scaling exponent, n, and the prefactor C. As indicated in Fig. 3, C and D, increasing indentation depth leads to increases in both n and C, which range in value from 2.4–2.7 and 0.7–1.1, respectively. Some variation for n and C is unsurprising given the more complicated deformation behavior of thick tubes; however, to a reasonable approximation, the scaling behavior and indentation behavior are described by Eq. 1. These data also indicate the range of reasonable values for n and C that might be expected for indentation of more-complex cylindrical structures like microtubules. Understanding reasonable ranges of values for n and C could also be useful for developing more-sophisticated mathematical models of microtubule indentation.

To examine more-realistic microtubule-like tubes, we modeled hollow cylinders with a roughly corrugated outer surface to closely represent the striated protofilament structure of microtubules. The skew and radius of these tubes were systematically varied to match the geometry of microtubules found in vitro (35). A summary of the 10 tubes modeled can be found in Table 1 and the results are shown in Fig. 4. This series of tubes allows simultaneous analysis of changes in radius, protofilament number, and skew, and examination of the sensitivity of AFM to the specific microtubule geometry during nanoindentation. For the geometries modeled, we find wide variability in the values of k_{MT}, with values ranging from 0.06 to 0.11 N/m (Fig. 4 *A*). More significantly, there is no obvious correlation between skew angle of the protofilaments and k_{MT}. However, when k_{MT} is considered only as a function of tube radius, scaling similar to that of a simple hollow cylinder is revealed, despite the different protofilament geometries. Defining k_{MT} as the average slope of these indentation data allows a least-squares fit to the modeling data, and we find that for an indentation depth of 3 nm, $n = 2.48 \pm 0.03$ and $C = 1.05 \pm 0.05$. This compares very favorably with the same values for thick-walled cylinders at this indentation depth.

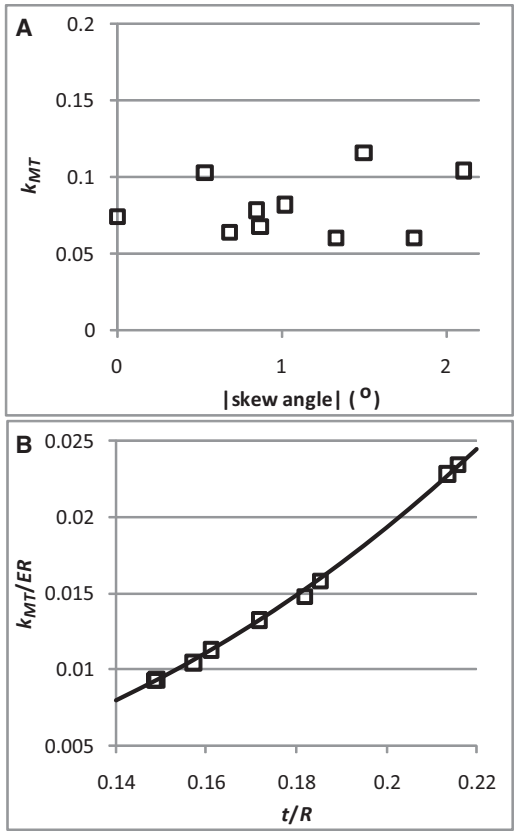

FIGURE 4 (*A*) Effective spring constant as a function of protofilament skew angle for the set of microtubule types described in Table 1. Values for k_{MT} were estimated using a linear fit after 3 nm of indentation. The relative standard error in the fits is ~3%, so error bars are smaller than the data points. (*B*) The same spring constant data normalized against radius and modulus and plotted against t/R. The line corresponds to a least-squares fit to the data using Eq. 1, where $n = 2.48 \pm 0.03$ and $C = 1.05 \pm 0.05$.

To further exclude the effects of skew on the measurement of k_{MT}, a set of tubes were modeled with constant radius ($R_{in} = 9.32$ nm) and with skew ranging from 0° to 2° (the range observed experimentally (33)). It should be noted that these tubes do not correspond to any known microtubule types; they were used to isolate the effect of skew alone. In these models, the indentation curves were nearly identical, with an average deviation in k_{MT} of <1% between tubes (data not shown). This is well below the error inherent in a typical AFM nanoindentation experiment, in agreement with the FEM results in Table 1, and confirms that skew is not a relevant factor in curve-to-curve or sample-to-sample variability in experimental AFM force curves. These results correlate well with previous descriptions of microtubule buckling during bending, where the helix start number does not affect the critical buckling force (27).

Our models do not take into account excess mechanical stress (prestress) that may accompany skewed protofilaments (33). For the small indentations modeled here, prestress should not affect microtubule response; it should only be a significant factor for microtubules stressed into the nonlinear elastic regime (15), such as that shown in Fig. 2 *C*. For higher applied forces in AFM experiments, excess mechanical stress in the microtubule lattice may impact properties such as the critical buckling force; however, our goal here was to examine only the elastic indentation response. Further, a previous study (35) that proposed the presence of prestress focused on microtubule samples in which 13_3 was the dominant type. In those samples, the observed distribution of microtubule types was hypothesized to be a result of mechanical stress-induced excess free energy. However, alternative stabilization methods result in distinct distributions of microtubule types, and likely affect bond structure, energetics, and stress distribution in the microtubule lattice (35,38–43). For example, in the case of GMPCPP stabilization compared to paclitaxel stabilization, the least excess stress could plausibly be 14_3 and 12_3, respectively.

The data presented here were also obtained from models in which the contacting surface between the microtubule and the substrate was modeled using a minimum of immobilized contact area. To determine the effect of contact surface on the radial stiffness, we also modeled a series of microtubules in which up to three of the bottom protofilaments were fixed in position, simulating microtubules that are more strongly immobilized to the underlying surface (see Fig. S1 in the Supporting Material). Even in these cases, the scaling described by Eq. 1 is maintained, albeit with values of n and C that are significantly higher than expected for thin shells. Thus, all of our models suggest that the dominant factor in determining microtubule radial stiffness in each of these experiments is the tube dimension (t/R) and not skew.

Our modeling results suggest that the subtle effect of protofilament skew is undetectable in AFM indentation experiments. The FEM results presented here and in previous works (13,15) offer clear evidence that microtubule radius and wall thickness are key factors in determining the radial stiffness. It follows that an important question to consider is whether the dimensions of microtubules measured in AFM accurately reflect their actual physical dimensions. In fact, it is difficult to directly and unambiguously assign microtubule types or dimensions using AFM data. The technique is notoriously unreliable for assigning the true lateral dimensions of objects with high aspect ratios, such as microtubules, due to convolutions with the AFM tip shape (45). Further, assignment of microtubule diameter based on height in AFM images may also be inaccurate because topographic information is convolved with the stiffness of objects under the tip; that is, under given load, stiffer objects appear taller. It may be feasible to directly assign protofilament skew from AFM images; indeed, in the best AFM images, with small image sizes and high spatial resolution, it is possible to resolve protofilaments on the top surface of the microtubule (15,46,47). However, distortions in AFM

images due to nonlinearities in the piezoelectric scanner or effects such as thermal drift make it difficult to definitively assign small skew angles ($<2^\circ$) without imaging the microtubule lattice over long distances. Although we have obtained images that resolve individual protofilaments, at present we have been unable to unambiguously assign protofilament skew from AFM data, and to our knowledge there have been no reports of direct assignment of the microtubule lattice type from AFM images.

Known distributions of microtubule types in solution could also provide an indirect avenue to deduce distributions of microtubule types that are surface-immobilized for an AFM experiment. The limitation in this approach is that AFM is perturbative by nature and likely biased toward more stable microtubule types. For example, 13_3 microtubules may be overrepresented (compared to solution) in AFM experiments due to their energetic stability and ability to withstand AFM imaging (15,35). Indeed, some previous AFM studies focused the description of microtubule indentation only on the prototypical 13_3 microtubule (15,16). This is the most common microtubule found in vivo, and it is the microtubule geometry most easily described computationally because it contains two symmetry planes that can be exploited to reduce the size of FEM calculations. For most microtubules prepared in vitro, however, paclitaxel is used as a stabilizing agent, and thus samples likely contain 12_3 microtubules as the predominant type (38,40,41). Additionally, 14_3 microtubules are also important to our work (14) because GMPCPP strongly induces their formation (43). Simply on the basis of the known distribution of microtubule types found in solution, it is reasonable to assume that AFM experiments with GMPCPP-stabilized microtubules are examining microtubules with different geometries than paclitaxel-stabilized samples. Additionally, the microtubule lattice type may vary within individual microtubules (34), and we have reported changes in microtubule diameter in AFM images (14) that were attributed to changes in protofilament number. Finally, the reported spread of measured microtubule radii and k_{MT} values in many AFM studies would indicate that several microtubule types are being sampled (14–16).

Although we cannot directly assign microtubule type in our microtubule samples using AFM, we can arrive at some reasonable hypotheses for the origin of the difference in stiffness observed for GMPCPP- compared to paclitaxel-stabilized microtubules. The FEM results presented in Fig. 4 indicate that the subtle effect of protofilament skew is undetectable in AFM indentation experiments, thus ruling out skew as a cause for changes in k_{MT}. The most obvious other geometric effects to consider are the tube radius or effective wall thickness. In the case of radius, we note that we observed with AFM that surface-immobilized GMPCPP microtubules have a larger average radius than paclitaxel microtubules (14), in qualitative agreement with a larger radius of 14-protofilament compared to 12-protofilament microtubules. However, according to Eq. 1, this should contribute to a decreased stiffness for GMPCPP microtubules and cannot explain the effect we observe. The stiffness variation we observe would require that the effective wall thickness change by a factor of ~1.5. At the single protein level, we interpret this as a change in number of intermolecular interactions across the interprotofilament interface. However, recent studies indicate that paclitaxel induces only subtle changes at the interprotofilament interface, caused by displacement of the M-loop, a 16-residue segment near the paclitaxel-binding site (48,49).

The final factor that could contribute to changes in indentation stiffness is a change in the effective Young's modulus of the polymeric tubulin material. This could plausibly come from a global change in the modulus of the protein, or from a change in effective stiffness local to regions of high stress. Our FEM models verify previous studies (15) that located most of the indentation-induced stress at the interprotofilament bridges (indicated in Fig. 1 *B*, *inset*). Binding of paclitaxel occurs near the interprotofilament interface and is the likely candidate for softening of this interface, causing a reduction in effective modulus. Recent studies have indicated that paclitaxel may reduce conformational flexibility of peptide chains local to its binding site, but it may simultaneously have a more global softening effect, increasing conformational flexibility in regions of the tubulin dimer distal to paclitaxel binding (48,49) and pointing to paclitaxel as a chemical agent capable of modifying the inherent modulus of tubulin. If this is the case, during AFM mechanical measurements, GMPCPP-stabilized microtubules may better represent the mechanics of native unstabilized microtubules than those using paclitaxel-stabilized microtubules. To confirm this effect, we are currently investigating unstabilized GTP-containing microtubules with AFM, which present unique challenges because of their inherent instability. Of similar importance is the correlation of specific microtubule type, skew, or radius with measured values of indentation stiffness. These types of experiments could directly corroborate the modeling results presented here and offer more detailed insight into microtubule mechanics.

Our results can also be compared with more macroscopic measurements of the bending of whole microtubules, which have produced a range of values for flexural rigidity. With appropriate simplifying assumptions about microtubule structure and physical properties, it is possible to use flexural rigidity values to estimate more general material properties such as Young's modulus. Most commonly, bending experiments are interpreted by describing microtubules as homogeneous isotropic hollow cylinders with a well-defined moment of inertia (For example, describing a microtubule as a cylindrical tube with an outer diameter of 25 nm and a 12.5 nm inner diameter results in a moment of inertia of 1.7×10^{-32} m^4.). With these considerations, most studies (2,5,8–10) report that paclitaxel decreases the effective

Young's modulus, whereas stabilization with microtubule associated proteins or GMPCPP increases the effective modulus (3,5,8,9). To our knowledge, only one bending study has directly compared paclitaxel-stabilized with GMPCPP-stabilized microtubules (3). That work reported a change in flexural rigidity by a factor of 1.8, which, if microtubules are treated as isotropic cylinders, would correspond to a change in the elastic modulus by the same amount. Indeed, if stabilization-induced changes in flexural rigidity are caused by changes in Young's modulus, the effect may be significant.

CONCLUSIONS

The FEM data presented above provide evidence that microtubules behave as simple hollow cylinders with walls of finite thickness during local radial indentation. They also indicate that the presence of protofilaments and their orientation have little or no effect on radial indentation data obtained with AFM. These results allow for improved interpretation of measurements of microtubule stiffness with AFM. Additionally, they allow us to examine published AFM data comparing paclitaxel- and GMPCPP-stabilized microtubules to deduce that differences in indentation stiffness are not brought about by subtle geometric changes. Future FEM models that eliminate protofilaments and simply use a thick-shell model will be able to provide an accurate description of microtubule deformation, significantly reducing the model size and computation time. Finally, our measurements suggest a net softening effect induced by paclitaxel that may be an important key to understanding the mechanism by which it stabilizes microtubules.

SUPPORTING MATERIAL

Two figures are available at http://www.biophysj.org/biophysj/supplemental/S0006-3495(10)00835-0.

The authors thank Dr. Teresa Garrett and Mr. Cristian Opazo for helpful discussions.

This study was supported by the Frances D. Fergusson Faculty Technology Exploration Fund, the Camille and Henry Dreyfus Foundation, the Research Corporation, and the National Institutes of Health (grant 1R15GM083256-01).

REFERENCES

1. Alberts, B., A. Johnson, …, P. Walter. 2002. Molecular Biology of the Cell. Garland, New York.
2. Venier, P., A. C. Maggs, …, D. Pantaloni. 1994. Analysis of microtubule rigidity using hydrodynamic flow and thermal fluctuations. *J. Biol. Chem.* 269:13353–13360.
3. Mickey, B., and J. Howard. 1995. Rigidity of microtubules is increased by stabilizing agents. *J. Cell Biol.* 130:909–917.
4. Gittes, F., B. Mickey, …, J. Howard. 1993. Flexural rigidity of microtubules and actin filaments measured from thermal fluctuations in shape. *J. Cell Biol.* 120:923–934.
5. Kurachi, M., M. Hoshi, and H. Tashiro. 1995. Buckling of a single microtubule by optical trapping forces: direct measurement of microtubule rigidity. *Cell Motil. Cytoskeleton.* 30:221–228.
6. Elbaum, M., D. Kuchnir Fygenson, and A. Libchaber. 1996. Buckling microtubules in vesicles. *Phys. Rev. Lett.* 76:4078–4081.
7. Kurz, J. C., and R. C. Williams, Jr. 1995. Microtubule-associated proteins and the flexibility of microtubules. *Biochemistry.* 34:13374–13380.
8. Felgner, H., R. Frank, and M. Schliwa. 1996. Flexural rigidity of microtubules measured with the use of optical tweezers. *J. Cell Sci.* 109: 509–516.
9. Felgner, H., R. Frank, …, M. Schliwa. 1997. Domains of neuronal microtubule-associated proteins and flexural rigidity of microtubules. *J. Cell Biol.* 138:1067–1075.
10. Kikumoto, M., M. Kurachi, …, H. Tashiro. 2006. Flexural rigidity of individual microtubules measured by a buckling force with optical traps. *Biophys. J.* 90:1687–1696.
11. Pampaloni, F., G. Lattanzi, …, E. Florin. 2006. Thermal fluctuations of grafted microtubules provide evidence of a length-dependent persistence length. *Proc. Natl. Acad. Sci. USA.* 103:10248–10253.
12. VanBuren, V., L. Cassimeris, and D. J. Odde. 2005. Mechanochemical model of microtubule structure and self-assembly kinetics. *Biophys. J.* 89:2911–2926.
13. de Pablo, P. J., I. A. T. Schaap, …, C. F. Schmidt. 2003. Deformation and collapse of microtubules on the nanometer scale. *Phys. Rev. Lett.* 91:098101.
14. Munson, K. M., P. G. Mulugeta, and Z. J. Donhauser. 2007. Enhanced mechanical stability of microtubules polymerized with a slowly hydrolyzable nucleotide analogue. *J. Phys. Chem. B.* 111:5053–5057.
15. Schaap, I. A. T., C. Carrasco, …, C. F. Schmidt. 2006. Elastic response, buckling, and instability of microtubules under radial indentation. *Biophys. J.* 91:1521–1531.
16. Schaap, I. A. T., B. Hoffmann, …, C. F. Schmidt. 2007. Tau protein binding forms a 1 nm thick layer along protofilaments without affecting the radial elasticity of microtubules. *J. Struct. Biol.* 158:282–292.
17. Vinckier, A., C. Dumortier, …, L. Hellemans. 1996. Dynamical and mechanical study of immobilized microtubules with atomic force microscopy. *J. Vac. Sci. Technol. B.* 14:1427–1431.
18. Kis, A., S. Kasas, …, L. Forró. 2002. Nanomechanics of microtubules. *Phys. Rev. Lett.* 89:248101.
19. Kasas, S., A. Kis, …, S. Catsicas. 2004. Mechanical properties of microtubules explored using the finite elements method. *ChemPhysChem.* 5:252–257.
20. Charras, G. T., and M. A. Horton. 2002. Determination of cellular strains by combined atomic force microscopy and finite element modeling. *Biophys. J.* 83:858–879.
21. Hansen, J. C., R. Skalak, …, A. Hoger. 1996. An elastic network model based on the structure of the red blood cell membrane skeleton. *Biophys. J.* 70:146–166.
22. Carrasco, C., A. Carreira, …, P. J. de Pablo. 2006. DNA-mediated anisotropic mechanical reinforcement of a virus. *Proc. Natl. Acad. Sci. USA.* 103:13706–13711.
23. Michel, J. P., I. L. Ivanovska, …, C. F. Schmidt. 2006. Nanoindentation studies of full and empty viral capsids and the effects of capsid protein mutations on elasticity and strength. *Proc. Natl. Acad. Sci. USA.* 103:6184–6189.
24. Kol, N., M. Gladnikoff, …, I. Rousso. 2006. Mechanical properties of murine leukemia virus particles: effect of maturation. *Biophys. J.* 91:767–774.
25. Tang, Y., G. Cao, …, Q. Cui. 2006. A finite element framework for studying the mechanical response of macromolecules: application to the gating of the mechanosensitive channel MscL. *Biophys. J.* 91:1248–1263.
26. Zhao, Y., K. Tamhane, …, J. Fang. 2008. Radial elasticity of self-assembled lipid tubules. *ACS Nano.* 2:1466–1472.

27. Hunyadi, V., D. Chrétien, …, I. M. Jánosi. 2007. Why is the microtubule lattice helical? *Biol. Cell.* 99:117–128.

28. Meurer-Grob, P., J. Kasparian, and R. H. Wade. 2001. Microtubule structure at improved resolution. *Biochemistry.* 40:8000–8008.

29. Nogales, E., M. Whittaker, …, K. H. Downing. 1999. High-resolution model of the microtubule. *Cell.* 96:79–88.

30. Li, H., D. J. DeRosier, …, K. H. Downing. 2002. Microtubule structure at 8 A resolution. *Structure.* 10:1317–1328.

31. Pierson, G. B., P. R. Burton, and R. H. Himes. 1978. Alterations in number of protofilaments in microtubules assembled in vitro. *J. Cell Biol.* 76:223–228.

32. Wade, R. H., D. Chrétien, and D. Job. 1990. Characterization of microtubule protofilament numbers. How does the surface lattice accommodate? *J. Mol. Biol.* 212:775–786.

33. Chrétien, D., and S. D. Fuller. 2000. Microtubules switch occasionally into unfavorable configurations during elongation. *J. Mol. Biol.* 298:663–676.

34. Chrétien, D., F. Metoz, …, R. H. Wade. 1992. Lattice defects in microtubules: protofilament numbers vary within individual microtubules. *J. Cell Biol.* 117:1031–1040.

35. Hunyadi, V., D. Chrétien, and I. M. Jánosi. 2005. Mechanical stress induced mechanism of microtubule catastrophes. *J. Mol. Biol.* 348:927–938.

36. Lanzavecchia, S., R. Dallai, …, B. A. Afzelius. 1991. The sperm tail of a gall midge and its microtubular arrangement studied by two strategies of image analysis (cecidomyiidae, diptera, insecta). *J. Struct. Biol.* 107:65–75.

37. Chalfie, M., and J. N. Thomson. 1982. Structural and functional diversity in the neuronal microtubules of Caenorhabditis elegans. *J. Cell Biol.* 93:15–23.

38. Andreu, J. M., J. Bordas, …, E. Towns-Andrews. 1992. Low resolution structure of microtubules in solution. Synchrotron X-ray scattering and electron microscopy of taxol-induced microtubules assembled from purified tubulin in comparison with glycerol and MAP-induced microtubules. *J. Mol. Biol.* 226:169–184.

39. Andreu, J. M., J. F. Díaz, …, J. Bordas. 1994. Solution structure of Taxotere-induced microtubules to 3-nm resolution. The change in protofilament number is linked to the binding of the taxol side chain. *J. Biol. Chem.* 269:31785–31792.

40. Arnal, I., and R. H. Wade. 1995. How does taxol stabilize microtubules? *Curr. Biol.* 5:900–908.

41. Díaz, J. F., J. M. Valpuesta, …, J. M. Andreu. 1998. Changes in microtubule protofilament number induced by Taxol binding to an easily accessible site. Internal microtubule dynamics. *J. Biol. Chem.* 273:33803–33810.

42. Dogterom, M., and B. Yurke. 1997. Measurement of the force-velocity relation for growing microtubules. *Science.* 278:856–860.

43. Hyman, A. A., D. Chrétien, …, R. H. Wade. 1995. Structural changes accompanying GTP hydrolysis in microtubules: information from a slowly hydrolyzable analogue guanylyl-(α,β)-methylene-diphosphonate. *J. Cell Biol.* 128:117–125.

44. Tortonese, M., and M. Kirk. 1997. Characterization of application-specific probes for SPMs. *Proc. SPIE.* 3009:53–60.

45. Hansma, H. G., and J. H. Hoh. 1994. Biomolecular imaging with the atomic force microscope. *Annu. Rev. Biophys. Biomol. Struct.* 23:115–139.

46. Schaap, I. A. T., P. J. de Pablo, and C. F. Schmidt. 2004. Resolving the molecular structure of microtubules under physiological conditions with scanning force microscopy. *Eur. Biophys. J.* 33:462–467.

47. Kacher, C. M., I. M. Weiss, …, M. Fritz. 2000. Imaging microtubules and kinesin decorated microtubules using tapping mode atomic force microscopy in fluids. *Eur. Biophys. J.* 28:611–620.

48. Mitra, A., and D. Sept. 2008. Taxol allosterically alters the dynamics of the tubulin dimer and increases the flexibility of microtubules. *Biophys. J.* 95:3252–3258.

49. Keskin, O., S. R. Durell, …, D. G. Covell. 2002. Relating molecular flexibility to function: a case study of tubulin. *Biophys. J.* 83:663–680.